Dopants and Traps in Nanocrystal-Based Semiconductor Thin Films: Origins and Measurement of Electronic Midgap States

Journal Article

Author(s):
Volk, Sebastian; Yazdani, Nuri; Yarema, Olesya; Yarema, Maksym; Wood, Vanessa

Publication date:
2020-02-25

Permanent link:
https://doi.org/10.3929/ethz-b-000397313

Originally published in:
ACS Applied Electronic Materials 2(2), https://doi.org/10.1021/acsaelm.9b00685

Dopants and Traps in Nanocrystal-based Semiconductor Thin Films: Origins and Measurement of Electronic Mid-Gap States

*Sebastian Volk, Nuri Yazdani, Olesya Yarema, Maksym Yarema, Vanessa Wood**

*Department of Information Technology and Electrical Engineering, ETH Zurich, Gloriastrasse 35, 8092 Zurich, Switzerland

Abstract

Different models are proposed to explain the origin of electronic mid-gap states that limit charge transport in nanocrystal thin films. Here, we investigate mid-gap states using optoelectronic and electrochemical techniques, supported by theoretical calculations. We find that charge trapping in PbS NC thin films can be explained by (1) nanocrystal dimerization and (2) charging of doped nanocrystals. In these models, there are no states within the bandgap of individual nanocrystals; the nanocrystals themselves act as trap states. These findings allow us to formulate strategies to improve transport by increasing free carrier densities while reducing the number density of trap states.

Keywords:

Nanocrystal thin films, PbS, trap state, electronic mid-gap state, Fourier Transform Photocurrent Spectroscopy, FTPS, Energy-Resolved Electrochemical Impedance Spectroscopy, ER-EIS

Colloidally synthesized nanocrystals (NCs) assembled into thin films hold promise for next generation semiconductors. The size-[1], shape-[1], composition-[2] and surface-termination[3] dependent characteristics of the NCs allow for wide tunability of semiconductor properties including the energies of the electronic states through which electron and hole transport occurs[4,5] as well as the electron and hole mobilities[6,7]. The performance of NC-based optoelectronic devices[8] however still fall short of what could be expected theoretically. Transport studies[9] reveal that this is in large part due to electronic deep-level trap states that reduce the effective mobility and act as efficient recombination centers[9–13]. Furthermore, although doping in NC thin films has been demonstrated[14], systematic approaches to control free carrier density and n- and p-type properties remain scarse[15].

A number of models now exist to explain the origin of traps states (see **Fig. 1**). (i) Deep-level states in NC semiconductors have typically been associated with electronic states that are located within the quantized electronic structure of individual NCs, in analogy to their bulk counterparts[16]. Some density functional theory (DFT) calculations suggest that physical defects at the NC surface (e.g. missing atoms, additional atoms, discoordinated surface atoms through ligand removal, atomic dimerization such as Pb-Pb formation at the NC surface) can give rise to these states[17–21]. (ii) NC dimerization (necking), observed in both solution-dispersed as well as crosslinked NCs[22,23], has also been identified as a trap state formation model[24]. Here, the electron (or hole) trap originates from the energy offset between the lowest unoccupied electronic state (highest occupied electronic state) of the dimerized NC and the surrounding NCs. The lower bandgap in the dimer result from the less pronounced confinement of the electronic wavefunction, which is centered in between the NC cores[24]. In this model, the entire dimer acts at the trap and the density of dimers is the density of electronic traps. Finally, (iii) mid-gap states

can arise due to charging of doped NCs within the NC solid[7]. Oxidation (reduction) of n-type (p-type) doped NCs shifts the entire electronic bandstructure of the NC. The energetic barrier presented by the energetic difference between the lowest unoccupied (highest occupied) electronic state of an n-type (p-type) charged NC and surrounding intrinsic NCs constitutes a trap state for electron (hole) transport. As in the dimer model (ii), in the charged NC model (iii), the trap-states are the quantum confined electronic states of individual NCs, and the number of trap states is linked to the number of oxidized (or reduced) doped NCs.

In both model (i) and model (iii), the presence of trap states is intimately linked to doping and free carrier generation in NC thin films. In the context of in-gap state models (**Fig 1(i)**), dopant atoms in NCs could form donor and acceptor states. Low performance metrics even upon high impurity concentrations have been associated with the large ionization energies needed to release the charges on the deep-level impurity states[7]. Charging models (as in **Fig 1(iii)**) take a completely different approach: here, free carrier generation is directly linked to the formation of deep-level trap states as a result of NC charging[7].

In this study, we investigate electronic mid-gap state formation using optoelectronic (Fourier Transform Photocurrent Spectroscopy, FTPS) and electrochemical (Energy-Resolved Electrochemical Impedance Spectroscopy, ER-EIS) techniques, and we support our findings by *ab initio* simulations (DFT). We show that these methods are self-consistent but that certain techniques are only sensitive to certain types of traps states. For complete characterization and understanding of the in-gap structure of NC solids, both experimental techniques must be applied. For the model system of PbS NC thin films investigated here (**SI1**), we find evidence of trap states stemming from both dimerization as well as trap states coming from the

oxidation/reduction model. We find no evidence for electronic states located within the quantized electronic structure of individual NCs. These finding have important implications for how we need to fabricate and design semiconducting thin films made from NCs.

We start by probing mid-gap states in PbS NC solids by FTPS, which enables quantification of the density of states (DOS) over a large range of signal-to-noise ratios (>9 orders of magnitude). It was developed to measure intra-band and defect-linked transitions in microcrystalline silicon[25], and has also been used to measure defect states in NC-based solids[10].

Fig 2a illustrates the experimental FTPS setup. A near-infrared (NIR) or mid-infrared (MIR) light source of a Fourier Transform Infrared (FTIR) spectrometer excites carriers across optically allowed transitions on individual NCs leading to a photocurrent across the device (**SI2** and **SI3**). Intensity-modulation of the light source (with a chopper) means that the excitation-induced photocurrent in the NC thin film will also exhibit a frequency dependence enabling it to be measured with lock-in techniques. After amplification through a transimpedance (TIA) and lock-in amplifier (LIA), the signal is fed back into the FTIR via the internal analog-to-digital converter for data processing. The total photocurrent I_{ph} is measured in reciprocal space as a function of optical path difference (**Fig 2b**). Fourier Transformation translates this interferogram pattern into a spectrally-resolved photocurrent density $J_{ph}(E)$ as shown in **Fig 2c** (solid line), normalized to the spectral intensity distribution of the incident beam source (**SI4, Part 1**). Since $J_{ph}(E)$ is derived through Fourier Transformation, the energy resolution is inversely proportional to the measured optical path difference range (all FTPS settings in **SI4, Part 2**). An estimate for the experimental resolution limit (derivation in **SI4, Part 1**) is shown with the dashed line (**Fig 2c**).

The photocurrent spectrum of a PbS:EDT thin film with Au-contacts (**Fig 2c, top)** consists of a main peak centered at E_G = 1.22 eV. This feature is associated with an optical transition from the highest occupied electronic state to the lowest unoccupied electronic state of the NC. Its energy position is slightly lower than the free exciton peak in solution at $E_{PbS}^{abs,sol}$ = 1.28 meV for these NCs (solution and thin film absorption profile in **SI5**) due to electronic coupling between NCs and a change in the dielectric constant of the medium surrounding the NCs (solution vs. NC-solid), which can lead to shifts in the bandgaps of up to 50 meV for bandgaps in the 1-1.5 eV range[5].

Within the sub-bandgap energy range, we observe a feature around 0.8 eV, 420 meV below the first exciton peak (**Fig 2c**), comparable to trap depths (**SI6**). In identifying the mid-gap feature in the FTPS measurement, we note that, to appear in a FTPS measurement, the transition must be optically allowed and the optically excited carriers must be able to be extracted electronically to the contacts.

With FTPS, trap states in a NC solid arising from the charging model (iii) will not be observable. The FTPS signal from the trap states in this model (which are themselves individual NCs) would also give rise to a signal at E_G and thus be indistinguishable from the signal from other NCs in this film (**Fig 2d**). Therefore, the charging model cannot explain the mid-gap feature seen in **Fig. 2c**.

Traps states arising due to dimerization model will be observable with FTPS, and indeed, mid-gap states, linked to dimerization, were observed at a similar energy depth by direct photoexcitation and transient absorption spectroscopy[24]. This study showed efficient electronic coupling and thermalization of carriers of the dimers to the neighboring NCs, which would also explain our ability to see such states with FTPS. DFT calculations indicate that a dimer formed from two PbS NCs with 1 eV bandgaps, will have a bandgap 160 meV smaller[24] (~840 meV), and dimers formed with the smaller NCs (with larger bandgap) studied here should experience an even more dramatic reduction in the bandgap. The sub-bandgap energy feature in the FTPS spectra could therefore be explained by excitation of the band-to-band transition on NC dimers, which have smaller net bandgaps (**Fig 1(ii)**).

With the data presented so far, an in-gap state model (**Fig 1(i)**) could also explain the existence of such a sub-bandgap feature. To rule-out the in-gap state model as an explanation for this feature, we perform measurement on an identical NC thin film with LiF/Al contacts (**Fig 2c, bottom)**. In contrast to Au contacts (with workfunction Φ_{Au} around 5.1 eV)[26], which lie close in energy to the highest occupied NC state, the work function of the Al contact (Φ_{Al} = 3.97 eV) decreases upon LiF deposition (down to $\Phi_{Al/(3\ nm\ LiF)}$ = 3.54 eV for thick LiF layers[27]. Here, partial LiF coverage results in an effective workfunction comparable to the energy position of the lowest unoccupied states of the NC at 3.67 eV[5]. In the case of LiF/Al contacts, any electronic state within the bandgap would be populated by electrons and the trap state feature at 0.8 eV would no longer be observable by FTPS. However, in the case of in-gap states, we would then expect a feature in the range 300-450 meV to emerge in the FTPS signal, corresponding to excitation of an electron in the trap state level to the lowest unoccupied electronic states (see **Fig.**

2d(i)). For the Al/LiF contacted film, the feature at 0.8 eV does disappear, but we do not observe a feature at 300-450 meV (**Fig 2c**). The in-gap state model (**Fig 1(i)**) therefore does not explain the results. In contrast, the dimer model is supported by the results on the Al/LiF (**Fig 2d**, (ii)). The lowest unoccupied electronic states of the dimers will be filled in the case of Al/LiF contacts, suppressing band-to-band transitions in the dimers as observed.

Thus, we conclude that (1) trap states measured in these PbS:EDT NC thin films exhibit electronic traps states coming from dimers and not states within the band gap of individual NCs, and that (2) performing FTPS on films contacted with different workfunction metals can be used to probe the different models for electronic trap states by selectively populating and depopulating them.

To investigate the formation of mid-gap electronic states due to doping, we consider bismuth (Bi)-doped PbS NCs. Bi atoms can be added to PbS NCs via post-synthetic cation exchange reactions[5,28], and, due to the higher number of valence electrons in Bi than Pb ($N_{e,Bi} = 5$ vs. $N_{e,Pb} = 4$), Bi-doped PbS lead to n-type behavior[28]. To date, Bi-doping of PbS has been associated with the creation of donor states within the bandgap of individual NCs (i.e., the formation of an in-gap state (**Fig 1**(**i**))[28,29]. This assumption seems to be supported by photoluminescence (PL) measurements on Bi-doped PbS solutions[29] and electrochemical measurements of the electronic structure of Bi-doped PbS thin films[28], which both show sub-bandgap features. However, DFT calculations and FTPS measurements highlight problems with the assumption of an in-gap model (**Fig 1**(**i**)) to explain heterovalent NC-doping and, as we will show, reconciliation of all data necessitates the introduction of the charge transfer model (**Fig 1**(**iii**)).

DFT calculations on isolated PbS and Bi-doped NCs are shown in **Fig 3a** (technical summary in **SI7**). Beyond symmetry breaking accompanied by a lifting of the degeneracies of the electronic onset states, our simulations predict only minor (sub 20 meV) changes of the electronic bandgap upon Bi-doping and show no additional states formed within the bandgap.

However, consistent with previous work, the photoluminescence (PL) of our Bi-doped PbS NCs dispersed in solution shows an emission feature at lower energy that is not present for the PbS NCs (**Fig 3b**). Transmission electron microscopy (TEM, **Fig 3c-d**, **SI8**) enables us to reconcile the seeming conflict between the DFT calculations (showing a clean NC bandgap) and solution PL (indicating a lower energy feature). While TEM of PbS NCs shows well-dispersed individual NCs (**Fig 3c**), after Bi doping, approximately 2-5% of the NCs in solutions are dimerized (**Fig 3d**). The energy spacing of the low energy PL feature relative to the main peak of the Bi-doped PbS NCs (270 meV) agrees with the decrease in bandgap that can be expected from dimerization. Dimerization of solvated Bi-doped PbS NCs, which creates a population of NC-dimers with lower bandgap, can thus explain why the solution PL measurements indicate the presence of sub-bandgap emission while DFT predicts a state-free bandgap.

Although the dimerization model explains the PL characteristics for solvated NCs, it is not sufficient to explain the combination of ER-EIS and FTPS measurements on thin films. The electronic density of states (DOS) of PbS NCs and Bi-doped PbS NC thin films measured electrochemically using ER-EIS are shown in **Fig 4a** (**SI9**).[5] The DOS of undoped PbS NC thin films (gray) shows a small trap state feature with an energy depth matching that of the dimer

feature in the FTPS spectra from **Fig 2c**. In contrast, the DOS of the Bi-doped NC film (blue) shows a dominant electronic mid-gap state manifold about $E_t^{ER\text{-}EIS}$ = 210 meV below the lowest unoccupied electronic states while the highest occupied electronic state onset remains unchanged.

In order to understand the origin of this mid-gap state in the Bi-doped PbS NC thin film, we first perform FTPS measurements, and, in **Fig 4b**, we plot the photocurrent for the PbS NC thin film (gray) and Bi-doped PbS NC thin film (blue). To compare the relative spectral signal intensity, the first exciton peak is normalized to 1 (raw data in **SI4, Part 1**). Both FTPS measurements coincide over the whole energy range from 0.1 to 1.5 eV. Gaussian fits to the features (in black) of doped and undoped NCs agree quantitatively in their energy position (μ_{PbS} = 0.80 eV vs $\mu_{Bi\text{-}PbS}$ = 0.78 eV), integrated relative current ($A_{PbS} = 3.7\cdot10^{-5}$ vs $A_{Bi:PbS} = 3.4\cdot10^{-5}$) and spread ($\sigma_{PbS}$ = 0.50 eV vs $\sigma_{Bi\text{-}PbS}$ = 0.64 eV). Differences lie within the experimental standard deviation of the measurements (see discussion in **SI10**). Due to the quantitative agreement between the FTPS on the doped and undoped samples, we link the feature in the Bi-PbS NCs to the occurrence of dimers as in the undoped PbS NC. While dimerization appears to occur in Bi-PbS NC solutions and not in PbS NC solutions, we conclude that the number density of dimers formed after crosslinking into a thin film is comparable for both NC species. This highlights that the extent of dimerization is highly dependent on the fabrication steps (and resulting surface properties) in agreement with previous reports[22–24]. With comparable dimer content in both films observed in FTPS, the dominant feature in ER-EIS spectra for doped NCs cannot be linked to dimerization.

We thus have an apparent contradiction: ER-EIS measurements show a mid-gap feature for Bi-doped PbS NCs while FTPS data does not. Since in-gap (**Fig 1(i)**) and dimerization models (**Fig1(ii)**) fail to explain this contradiction, we turn to charge state models (**Fig 1(iii)**). Large-scale DFT simulations on NC solids show that charging (oxidation/reduction) of doped NCs embedded in a NC network can act as a source of deep electronic states[7]. We simulate the effect of Bi-doping on the electronic structure of PbS NC solids (**SI7**). Doping of an individual NC does not cause a shift of its energy levels relative to those of its neighbors (**Fig 4c,** left-hand side and center). However, oxidation of the doped-NC results in a lowering of its entire electronic structure (**Fig 4c,** right hand side). For the particular NC size studied here, we calculate a shift of $E_t^{LS\text{-}DFT}$ = 215 meV[7], which is in agreement with mid-gap feature observed electrochemically ($E_t^{ER\text{-}EIS}$ = 210 meV). Furthermore, this charge transfer model explains why the highest occupied electronic state extracted out of the DOS spectra (and thus, the associated transport "valence band (VB)") onset remains the same as for the undoped NCs. The Bi-doped PbS NC thin film likely consists of oxidized doped NCs $(n\text{-NCs})^+$, non-oxidized doped NCs $(n\text{-NCs})^0$, and intrinsic NCs. The highest occupied electronic state onset arising from the latter two species of NC will coincide with that of the undoped NCs.

The charge transfer model thus resolves the apparent contradiction between the electrochemical and FTPS measurements. FTPS measurements will show energies of optically-active transitions occurring between sets of discrete energy levels. Due to the fact that this oxidation-induced shift leaves the bandgap almost unaffected, both intrinsic and charged Bi-doped NCs exhibit band-to-band transitions with first exciton peaks at E_G. The FTPS traces are thus expected to be the same as seen in **Fig 4b**, while electrochemical measurements will resolve the absolute shifts in energy.

In summary, we use a set of complementary experimental techniques and simulation to obtain a self-consistent explanation for the origin of trap states and doping in NC thin films. We do not find evidence of in-gap states within the quantized electronic structure of individual NCs. Our framework is capable of explaining phenomena that have been observed to date on EDT-functionalized PbS NCs without the need of such an in-gap model. Trapping and doping can instead be explained by dimerization and charging. We showed that doped and undoped NCs exhibit dimerization under certain preparation conditions, leading to populations of NC dimers with smaller bandgaps, which can act as trap states. Furthermore, we showed that while electronic levels of doped-NCs do not change dramatically from those of undoped-NCs, they shift relative to their neighboring NCs when oxidized (or reduced), leading to electronic trap states.

These results emphasize two important conclusions. First, we show the benefit of using a number of complementary techniques when exploring novel material systems and the importance of careful assessment of the measurement technique capabilities. In contrast to bulk semiconductors for which many of the methods for measuring traps and dopant have been developed, in the case of NCs, trap states and dopant states come from entire individual NC or NC dimers, which has the effect that doping-induced shifts of the electronic structure will be visible in electrochemical assessment, but not in optical or optoelectronic experiments.

Second, these observations provide clear insights into how to reduce trap state formation that is detrimental to charge carrier transport and address the low doping (i.e., free carrier formation)

efficiency in NC solids. Dimerization must be avoided through selection of surface treatment that stabilize NCs surface while also enabling good packing and electronic coupling between NCs. Doping of NCs should be done on NCs with different sized bandgaps[7], such that ionization barriers are low and that oxidation (or reduction) shifts the electronic states of the doped NC to align with those of the neighboring NCs.

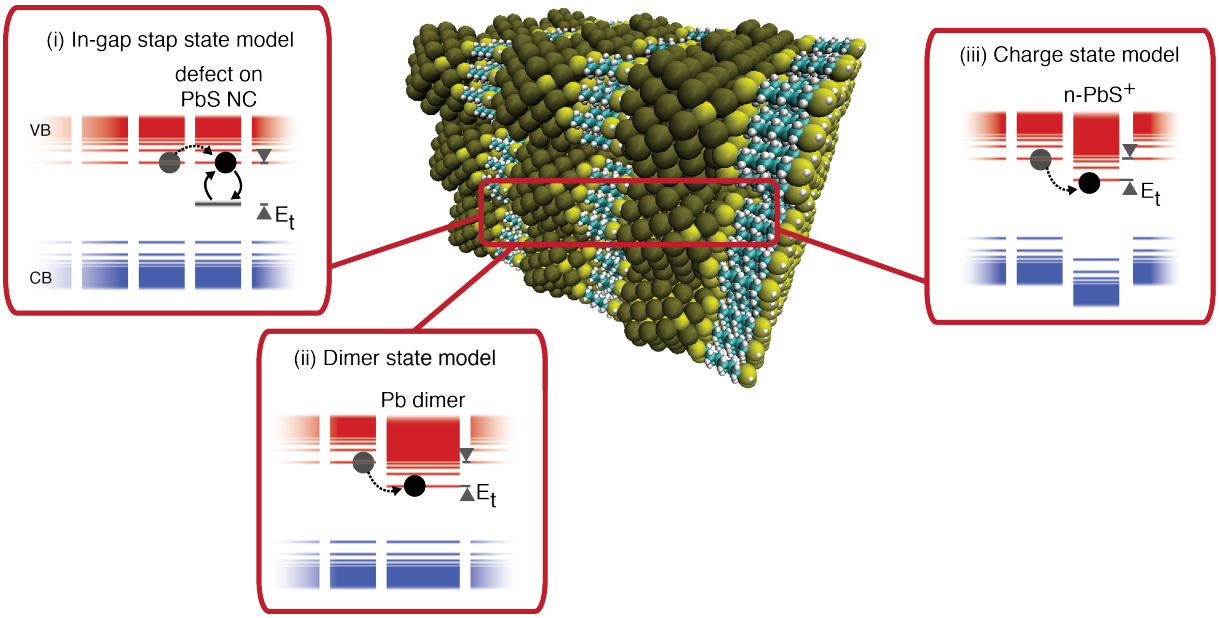

Figure 1. Schematic presentation of proposed trap state formation models in nanocrystal (NC) solids. (i) In-gap state models assume that an electronic state exists within the band-gap of individual NCs at a depth, E_t. (ii) Dimerization models are based upon changes of the quantized electronic structure as a result of two NCs fusing together (necking). The electron (or hole) trap comes from the energy difference between the lowest unoccupied (highest occupied) electronic state of the dimer and the neighboring monomers. (iii) Charge state models are based upon a shift of the entire electronic structure of the NC as a result of oxidation or reduction of doped (i.e. not charge neutral) NCs.

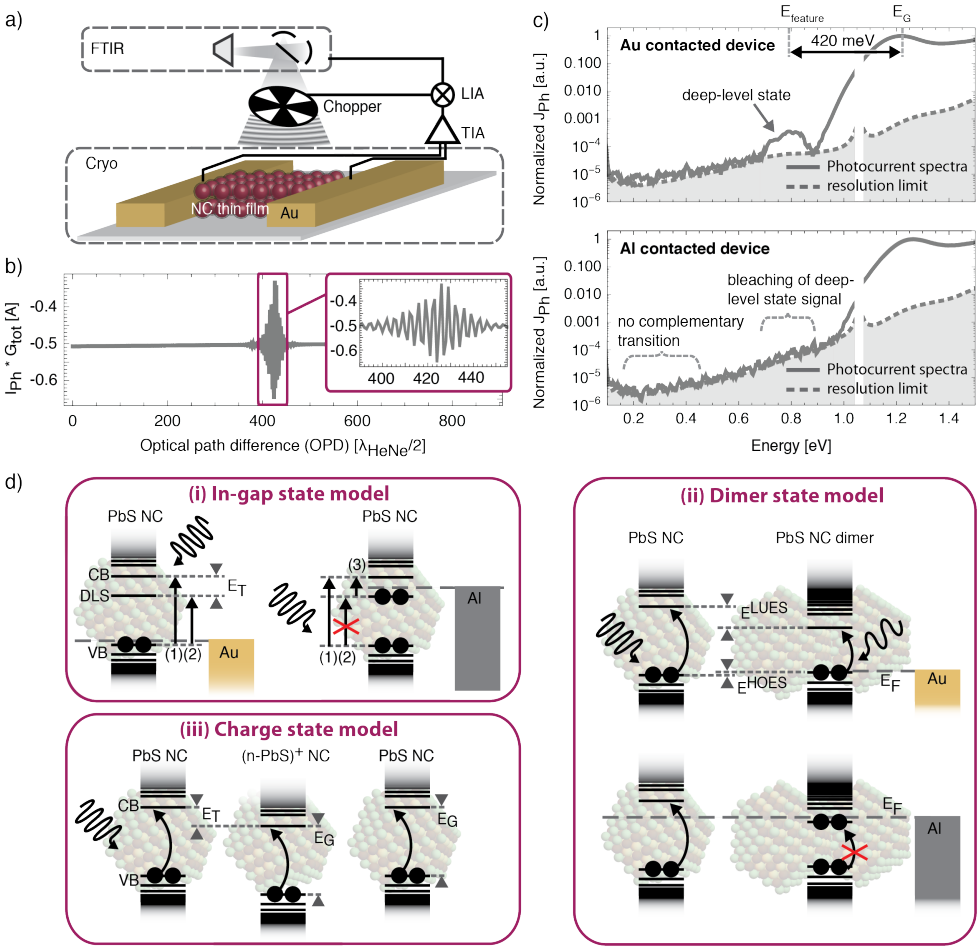

Figure 2. Measurement of trap states in PbS:EDT nanocrystal (NC) solids. a) Sketch of a Fourier Transform Photocurrent Spectroscopy (FTPS) setup. b) Typical FTPS measurements on PbS NC solids, recorded as a function of optical path difference showing an interferogram pattern due to wavelength-dependent interference. (c) Top: FTPS spectra (solid gray line) from a NC solid contacted with Au showing evidence of a deep level state. The resolution limit estimate is indicated in gray shading. Bottom: The mid-gap feature bleaches in FTPS measurements performed on the same film contacted to Al/LiF electrodes. d) Sketch of the electronic structure in a NC thin film and optical transitions contributing to a FTPS spectrum. (i) In-gap models (assuming a deep level state (DLS) at an energy depth E_T) fail to explain FTPS spectra on Al/LiF device structures as low-energy transitions are not present. (iii) Charge state models do not result in FTPS mid-gap states as charged and doped NCs only shift in energy, with their bandgap remaining unchanged. Only (ii) dimerization can explain an in-gap signal feature in FTPS stemming from a band-to-band transition of a NC dimer. Considering the occupation of states explains why the work function of the contact determines whether trap states are visible in FTPS.

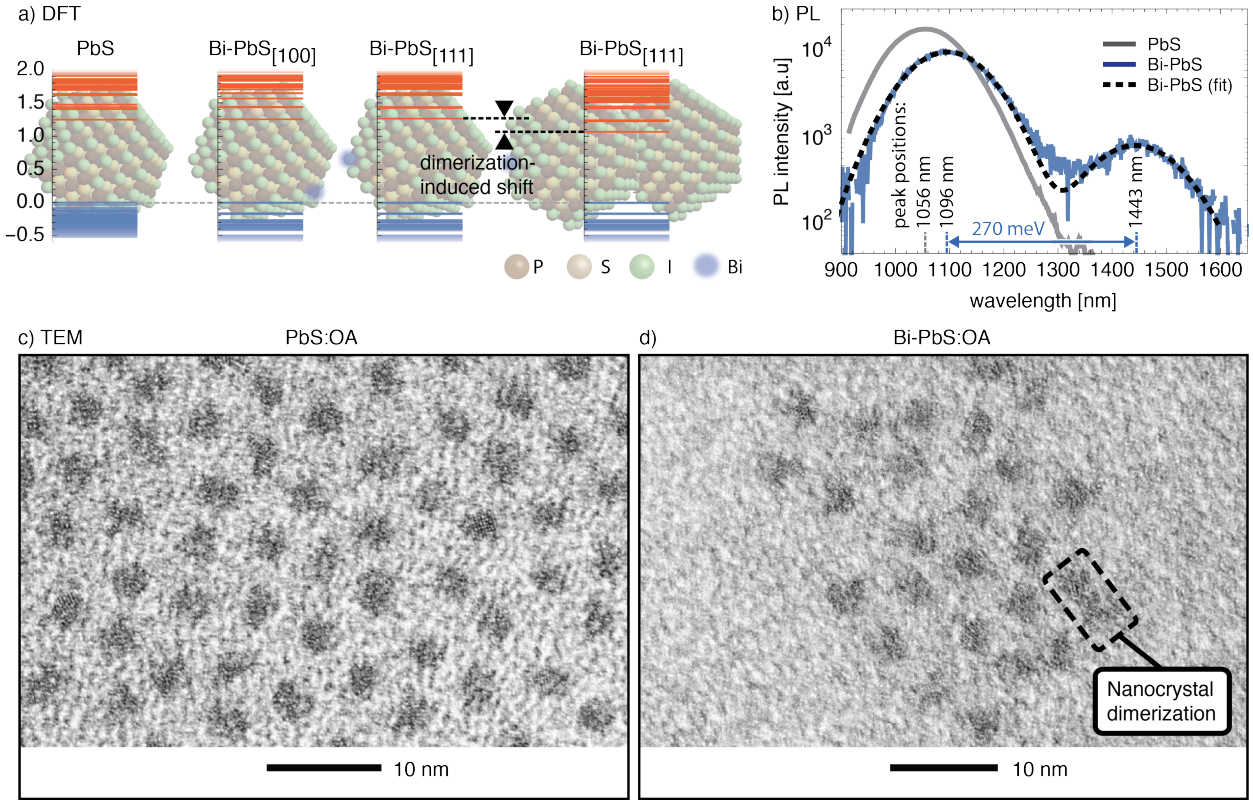

Figure 3. Doping-induced dimerization of individual nanocrystals (NCs): a) Density functional theory (DFT) calculations on individual NCs predict that Bi-doping (with Bi-replaced Pb atoms at the [100] or [111] surface of the NC, respectively) results in a symmetry-breaking of the electronic wavefunctions, accompanied by small shifts of the individual states (ΔE_G < 20 meV). In particular, no additional states within the bandgap are formed through Bi-doping. Bi-induced dimers are represented to the right, with the value of the band gap shrinkage taken from Ref [24], adapted for the size of our NC batch. The highest occupied electronic state is set to zero for better comparison. b) Photoluminescence studies of doped and undoped NCs in solution. Both NC species show an emission signal centered (fit) at 1056 nm (1.17 eV, PbS) and 1096 nm (1.13 eV, Bi-PbS), respectively. Furthermore, we observe a sub-bandgap energy emission feature at 1443 nm (0.86 eV) in the doped case, which we link to the emission of NC dimers. Contrast-enhanced TEM pictures of c) PbS NCs and d) Bismuth (Bi)-doped PbS NCs, surface-terminated with oleic acid. Whereas the reference NCs are only present as monomers, we observe dimerization in approx. 2-5% of doped NCs.

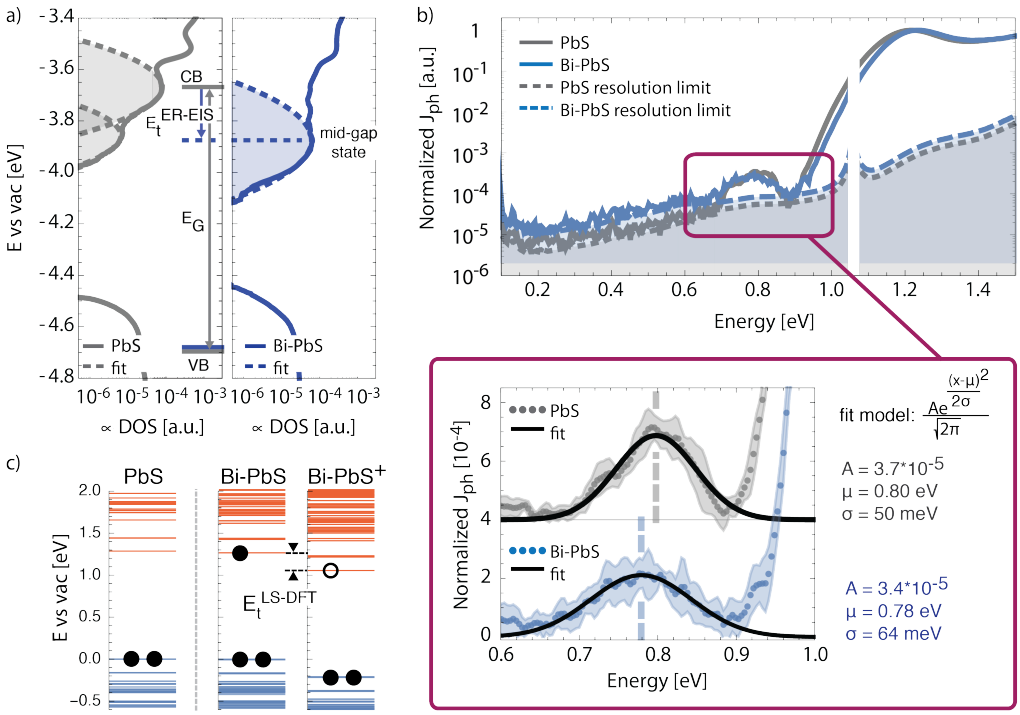

Figure 4. Understanding the electronic structure in Bi-doped PbS nanocrystal solids. a) Density of states (DOS) of undoped PbS (gray, left) and Bi-doped PbS (blue, right) NC solids, derived by Energy-Resolved Electrochemical Impedance Spectroscopy (ER-EIS). A Bi-induced feature emerges at E_t^{ER-EIS} = 210 meV below the lowest unoccupied electronic state of the reference thin film. Mean energy positions of Gaussian fits to the DOS features are labeled as conduction band (CB) and valence band (VB). Reproduced from Ref [5]. Copyright 2018 American Chemical Society. b) Top: Intensity-normalized photocurrent spectra measured by Fourier Transform Photocurrent Spectroscopy (FTPS) on PbS (gray) and Bi-doped PbS (blue) thin films embedded within gold contacts. One distinct feature at sub-bandgap energies is observed within the resolution limits (doted and dashed lines) for both NC assemblies at 0.78 - 0.80 eV. Bottom: A zoom-in on the sub-bandgap feature, with experimental mean values (dots), Gaussian fit (solid, black) and experimental standard deviation (shaded areas). The extracted parameters of the fits (right) for both doped and undoped NC species agree within the experimental standard deviation. The PbS trace is shifted for clarity. c) Large-scale density functional theory (LS-DFT) calculations predicting the electronic structure of individual NCs, embedded in a larger NC-network. Oxidation of doped NCs results in a downshift of the electronic structure by E_t^{LS-DFT} = 215 meV. This shift has recently (Ref [7]) been described as a source of electron trap state formation.

Supporting Information:

SI1: NC synthesis; **SI2:** Substrate preparation for FTPS; **SI3:** Thin film deposition; **SI4**, Fourier-Transform Photocurrent Spectroscopy (FTPS) on NC thin films; **Part 1**: FTPS methodology; **Part 2**: Experimental settings; **Part 3**: All FTPS raw data; **SI5**, Nanocrystal solution vs FTPS spectra; **SI6,** Comparison of trap depth measured by different techniques; **SI7:** DFT; **SI8:** TEM; **SI9:** Energy-resolved electrochemical impedance spectroscopy; **SI10**, Quantification of FTPS in-gap feature;

Author Information:

Corresponding author: *Email: vwood@ethz.ch

Author Contributions: SV performed the optoelectronic and electrochemical experiments. NY performed density functional theory calculations. OY and MY synthesized the material and took the TEM images. The manuscript was written through contributions of all authors. All authors have given approval to the final version of the manuscript.

Notes: The authors declare no financial interest.

Acknowledgements:

The authors gratefully acknowledge funding from the Swiss National Science Foundation through Sinergia (project CRSII2_147615) and the NCCR Quantum Science and Technology. We thank Daniel Burri for designing a FTPS sample holder and Vladimir Ovuka for assistance in the photolithography steps during substrate preparation.

Abbreviations:

NC, nanocrystal; DFT, density functional theory; FTPS, Fourier Transform Photocurrent Spectroscopy; ER-EIS, Energy-Resolved Electrochemical Impedance Spectroscopy; NIR, near-infrared; MIR, mid-infrared; FTIR, Fourier Transform Infrared; TIA, transimpedance amplifier; LIA, lock-in amplifier; PbS, lead sulfide; EDT, 1,2-Ethanedithiol; Au, gold; Al, aluminum; LiF, lithium fluoride; TAS, Thermal Admittance Spectroscopy; W, workfunction; eV, electron volt; Bi, bismuth; V, valence; PL, photoluminescence; TEM, Transmission electron microscopy; DOS, density of states;

References:

(1) Talapin, D. V; Lee, J.-S.; Kovalenko, M. V; Shevchenko, E. V. Prospects of Colloidal Nanocrystals for Electronic and Optoelectronic Applications. *Chem. Rev.* **2010**, *110*, 389–458.

(2) Yarema, O.; Yarema, M.; Lin, W. M. M.; Wood, V. Cu-In-Te and Ag-In-Te Colloidal Nanocrystals with Tunable Composition and Size. *Chem. Commun.* **2016**, *52*, 10878–10881.

(3) Boles, M. A.; Ling, D.; Hyeon, T.; Talapin, D. V. The Surface Science of Nanocrystals. *Nat. Mater.* **2016**, *15*, 141–153.

(4) Brown, P. R.; Kim, D.; Lunt, R. R.; Zhao, N.; Bawendi, M. G.; Grossman, J. C.; Bulović, V. Energy Level Modification in Lead Sulfide Quantum Dot Thin Films through Ligand Exchange. *ACS Nano* **2014**, *8*, 5863–5872.

(5) Volk, S.; Yazdani, N.; Sanusoglu, E.; Yarema, O.; Yarema, M.; Wood, V. Measuring the Electronic Structure of Nanocrystal Thin Films Using Energy-Resolved Electrochemical Impedance Spectroscopy. *J. Phys. Chem. Lett.* **2018**, 9, 1384–1392.

(6) Yazdani, N.; Bozyigit, D.; Yarema, O.; Yarema, M.; Wood, V. Hole Mobility in Nanocrystal Solids as a Function of Constituent Nanocrystal Size. *J. Phys. Chem. Lett.* **2014**, *5*, 3522–3527.

(7) Yazdani, N.; Andermatt, S.; Yarema, M.; Farto, V.; Bani-Hashemian, M. H.; Volk, S.; Lin, W.; Yarema, O.; Luisier, M.; Wood, V. Charge Transport in Semiconductors Assembled from Nanocrystals. *arXiv:*1909.09739v1 **2019**.

(8) Kagan, C. R.; Lifshitz, E.; Sargent, E. H.; Talapin, D. V. Building Devices from Colloidal Quantum Dots. *Science* **2016**, *353*, aac5523-aac5523.

(9) Bozyigit, D.; Lin, W. M. M.; Yazdani, N.; Yarema, O.; Wood, V. A Quantitative Model for Charge Carrier Transport, Trapping and Recombination in Nanocrystal-Based Solar Cells. *Nat. Commun.* **2015**, *6*, 1–10.

(10) Bozyigit, D.; Volk, S.; Yarema, O.; Wood, V. Quantification of Deep Traps in Nanocrystal Solids, Their Electronic Properties, and Their Influence on Device Behavior. *Nano Lett.* **2013**, *13*, 5284–5288.

(11) Nagpal, P.; Klimov, V. I. Role of Mid-Gap States in Charge Transport and Photoconductivity in Semiconductor Nanocrystal Films. *Nat. Commun.* **2011**, *2*, 486.

(12) Yoon, W.; Boercker, J. E.; Lumb, M. P.; Placencia, D.; Foos, E. E.; Tischler, J. G. Enhanced Open-Circuit Voltage of PbS Nanocrystal Quantum Dot Solar Cells. *Sci. Rep.* **2013**, *3*, 1–7.

(13) Luther, J. M.; Law, M.; Beard, M. C.; Song, Q.; Reese, M. O.; Ellingson, R. J.; Nozik, A. J. Schottky Solar Cells Based on Colloidal Nanocrystal Films. *Nano Lett.* **2008**, *8*, 3488–3492.

(14) Rivest, J. B.; Jain, P. K. Cation Exchange on the Nanoscale: An Emerging Technique for New Material Synthesis, Device Fabrication, and Chemical Sensing. *Chem. Soc. Rev.* **2013**, *42*, 89–96.

(15) Kagan, C. R. Flexible Colloidal Nanocrystal Electronics. *Chem. Soc. Rev.* **2019**, *48*, 1626–1641.

(16) Katsiev, K.; Ip, A. H.; Fischer, A.; Tanabe, I.; Zhang, X.; Kirmani, A. R.; Voznyy, O.; Rollny, L. R.; Chou, K. W.; Thon, S. M.; Carey, G. H.; Cui, X.; Amassian, A.; Dowben,

P.; Sargent, E. H.; Bakr, O. M. The Complete In-Gap Electronic Structure of Colloidal Quantum Dot Solids and Its Correlation with Electronic Transport and Photovoltaic Performance. *Adv. Mater.* **2014**, *26*, 937–942.
(17) Houtepen, A. J.; Hens, Z.; Owen, J. S.; Infante, I. On the Origin of Surface Traps in Colloidal II–VI Semiconductor Nanocrystals. *Chem. Mater.* **2017**, *29*, 752–761.
(18) Ip, A. H.; Thon, S. M.; Hoogland, S.; Voznyy, O.; Zhitomirsky, D.; Debnath, R.; Levina, L.; Rollny, L. R.; Carey, G. H.; Fischer, A.; Kemp, K. W.; Kramer, I. J.; Ning, Z.; Labelle, A. J.; Chou, K. W.; Amassian, A.; Sargent, E. H. Hybrid Passivated Colloidal Quantum Dot Solids. *Nat. Nanotechnol.* **2012**, *7*, 577–582.
(19) Giansante, C.; Infante, I. Surface Traps in Colloidal Quantum Dots: A Combined Experimental and Theoretical Perspective. *J. Phys. Chem. Lett.* **2017**, *8*, 5209–5215.
(20) Du Fossé, I.; Ten Brinck, S.; Infante, I.; Houtepen, A. J. Role of Surface Reduction in the Formation of Traps in N-Doped II-VI Semiconductor Nanocrystals: How to Charge without Reducing the Surface. *Chem. Mater.* **2019**, *31*, 4575–4583.
(21) Voznyy, O.; Thon, S. M.; Ip, A. H.; Sargent, E. H. Dynamic Trap Formation and Elimination in Colloidal Quantum Dots. *J. Phys. Chem. Lett.* **2013**, *4*, 987–992.
(22) Hanrath, T.; Veldman, D.; Choi, J. J.; Christova, C. G.; Wienk, M. M.; Janssen, R. A. J. PbSe Nanocrystal Network Formation during Pyridine Ligand Displacement. *ACS Appl. Mater. Interfaces* **2009**, *1*, 244–250.
(23) Evers, W. H.; Goris, B.; Bals, S.; Casavola, M.; De Graaf, J.; Roij, R. Van; Dijkstra, M.; Vanmaekelbergh, D. Low-Dimensional Semiconductor Superlattices Formed by Geometric Control over Nanocrystal Attachment. *Nano Lett.* **2013**, *13*, 2317–2323.
(24) Gilmore, R. H.; Liu, Y.; Shcherbakov-wu, W.; Dahod, N.; Lee, E.; Weidman, M.; Li, H.; Jean, J.; Bulovic, V.; Willard, A.; Grossman, J. C.; Tisdale, W. A. Epitaxial Dimers and Auger-Assisted De-Trapping in PbS Quantum Dot Solids. *Matter* **2019**, *1*, 250–265.
(25) Vanecek, M.; Poruba, A. Fourier-Transform Photocurrent Spectroscopy of Microcrystalline Silicon for Solar Cells. *Appl. Phys. Lett.* **2002**, *80*, 719–721.
(26) Haynes, W. M. *CRC Handbook of Chemistry and Physics*; Taylor & Francis: New York, 2008.
(27) Volk, S.; Yazdani, N.; Yarema, O.; Yarema, M.; Bozyigit, D.; Wood, V. In Situ Measurement and Control of the Fermi Level in Colloidal Nanocrystal Thin Films during Their Fabrication. *J. Phys. Chem. Lett.* **2018**, *9*, 7165–7172.
(28) Stavrinadis, A.; Rath, A. K.; García De Arquer, F. P.; Diedenhofen, S. L.; Magén, C.; Martinez, L.; So, D.; Konstantatos, G. Heterovalent Cation Substitutional Doping for Quantum Dot Homojunction Solar Cells. *Nat. Commun.* **2013**, *4*, 1–7.
(29) Papagiorgis, P.; Stavrinadis, A.; Othonos, A.; Konstantatos, G.; Itskos, G. The Influence of Doping on the Optoelectronic Properties of PbS Colloidal Quantum Dot Solids. *Sci. Rep.* **2016**, *6*, 1–16.

Charge carrier trapping in nanocrystal solids

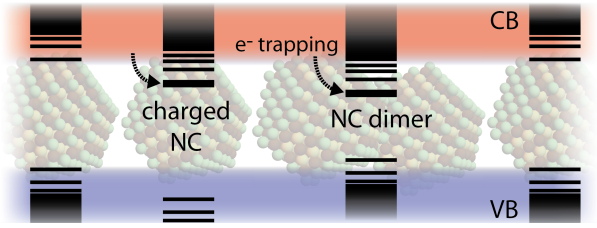

TOC